

Thu. Oct 27, 2022

Room-F

Interenational sess.

[1F07] Interenational sess. (1)

Chair:Shinya Furukawa(Hokkaido Univ.)

1:00 PM - 1:30 PM Room-F (13A Conf. room)

[1F07] [Invited] Nano-metal phosphides as green sustainable hydrogenation catalysts

○Takato Mitsudome<sup>1,2</sup> (1. Osaka University, 2. PRESTO)

1:00 PM - 1:30 PM

Interenational sess.

[1F08-1F11] Interenational sess. (2)

Chair:Shun Nishimura(National Inst. of Advanced Industrial Science &Technology)

1:30 PM - 2:30 PM Room-F (13A Conf. room)

[1F08] Protection strategy for selective oxidative esterification of HMF-dimethylacetal to dimethylfuran-2,5-dicarboxylate with Au/CeO<sub>2</sub>

○Nirupama Sheet<sup>1</sup>, Jan J. Wiesfeld<sup>1</sup>, Atsushi Fukuoka<sup>1</sup>, Kiyotaka Nakajima<sup>1</sup> (1. Institute for Catalysis, Hokkaido University)

1:30 PM - 1:45 PM

[1F09] Stereospecific ring opening metathesis polymerization of cyclic olefins by vanadium-alkylidene catalysts containing N-heterocyclic carbene ligands

○Jirapa Suthala<sup>1</sup>, Kotohiro Nomura<sup>1</sup> (1. Tokyo Metropolitan University)

1:45 PM - 2:00 PM

[1F10] Synthesis of bio-based network polymers by acyclic diene metathesis polymerization

○Lance O'Hari P. Go<sup>1</sup>, Kotohiro Nomura<sup>1</sup> (1. Tokyo Metropolitan University)

2:00 PM - 2:15 PM

[1F11] Conversion of *N*-acetylglucosamine derived from marine biomass chitin over ion-exchanged montmorillonite

○Kiyoyuki Yamazaki<sup>1</sup>, Norihito Hiyoshi<sup>1</sup>, Aritomo Yamaguchi<sup>1</sup> (1. The National Institute of Advanced Industrial Science and Technology(AIST))

2:15 PM - 2:30 PM

Interenational sess.

[1F12-1F14] Interenational sess. (3)

Chair:Yasutaka Kuwahara(Osaka Univ.)

2:45 PM - 3:45 PM Room-F (13A Conf. room)

[1F12] [Invited] Low-dimensional assembling of iron-aqua complexes for designing post-TiO<sub>2</sub>

○Yusuke Ide<sup>1</sup> (1. National Institute for Materials Science, International Center for Materials Nanoarchitectonics)

2:45 PM - 3:15 PM

[1F13] Development of thermally stable highly dispersed supported polyoxometalate cesium salts

○Takaaki Suzuki<sup>1</sup>, Tomohiro Yabe<sup>1</sup>, Keiju Wachi<sup>1</sup>, Kentaro Yonesato<sup>1</sup>, Kosuke Suzuki<sup>1</sup>, Kazuya Yamaguchi<sup>1</sup> (1. the University of Tokyo)

3:15 PM - 3:30 PM

[1F14] Crystalline Zr<sub>3</sub>SO<sub>9</sub> oxides with superior acid catalytic property to the conventional sulfated zirconia

○Meilin Tao<sup>1</sup>, Satoshi Ishikawa<sup>1</sup>, Takuji Ikeda<sup>2</sup>, Shunsaku Yasumura<sup>3</sup>, Yuan Jing<sup>3</sup>, Takashi Toyao<sup>3</sup>, Ken-ichi Shimizu<sup>3</sup>, Hiromi Matsuhashi<sup>4</sup>, Wataru Ueda<sup>1</sup> (1. Kanagawa University, 2. Research Institute for Chemical Process Technology, National Institute of Advanced Industrial Science and Technology (AIST), 3. Institute for Catalysis, Hokkaido University, 4. Hokkaido University of Education)

3:30 PM - 3:45 PM

Fri. Oct 28, 2022

Room-F

Interenational sess.

[2F01-2F04] Interenational sess. (4)

Chair:Naohiro Shimoda(Tokushima Univ.)

9:00 AM - 10:00 AM Room-F (13A Conf. room)

[2F01] CeO<sub>2</sub>-supported bimetallic Ni-Ag catalyst for ammonia synthesis from NO-CO-H<sub>2</sub>O

Chandan Chaudhari<sup>1</sup>, ○Yuichi Manaka<sup>1,2</sup>, Tetsuya Nanba<sup>1</sup> (1. Fukushima Renewable Energy Institute, AIST, 2. School of Materials and Chemical Technology, Tokyo Institute of Technology)

9:00 AM - 9:15 AM

[2F02] Plasmon-assisted hydrogenation and dehydrogenation reactions of noble metal nanoparticles

○Priyanka Verma<sup>1</sup>, Kohsuke Mori<sup>2</sup>, Yasutaka

Kuwahara<sup>2</sup>, Ryo Watanabe<sup>1</sup>, Hiromi Yamashita<sup>2</sup>, Choji  
Fukuhara<sup>1</sup> (1. Shizuoka University, 2. Osaka  
University)

9:15 AM - 9:30 AM

[2F03] Effect of Ca addition on the catalytic activity  
of BaTiO<sub>3</sub> for oxidative coupling of methane

○Rongguang Gan<sup>1</sup>, Yoshihide Nishida<sup>1</sup>, Masaki  
Haneda<sup>1</sup> (1. Nagoya Institute of Technology)

9:30 AM - 9:45 AM

[2F04] CO<sub>2</sub> hydrogenation reaction over Pd-containing  
MWW zeolite catalyst

○Willie Yang<sup>1</sup>, Shuhei Yasuda<sup>1</sup>, Sridharan Balu<sup>2</sup>,  
Muyuan Yu<sup>1</sup>, Toshiki Kaseguma<sup>1</sup>, Toshiyuki Yokoi<sup>1</sup> (1.  
Tokyo Institute of Technology, 2. National Taipei  
University of Technology)

9:45 AM - 10:00 AM

---

Interenational sess.

[2F05-2F07] Interenational sess. (5)

Chair:Ryo Watanabe(Shizuoka Univ.)

10:15 AM - 11:15 AM Room-F (13A Conf. room)

---

[2F05] Direct synthesis of carbamates as polyurethane  
raw materials from low-concentration of CO<sub>2</sub>  
equivalent to thermal power plant exhaust gas

○Hiroki Koizumi<sup>1</sup>, Katsuhiko Takeuchi<sup>1</sup>, Kazuhiro  
Matsumoto<sup>1</sup>, Norihisa Fukaya<sup>1</sup>, Kazuhiko Sato<sup>1</sup>,  
Masahito Uchida<sup>2</sup>, Seiji Matsumoto<sup>2</sup>, Satoshi Hamura<sup>2</sup>,  
Jun-Chul Choi<sup>1</sup> (1. National Institute of Advanced  
Industrial Science and Technology , 2. Tosoh

Corporation)

10:15 AM - 10:30 AM

[2F06] Design of efficient catalyst for higher alcohols  
synthesis via CO<sub>2</sub> hydrogenation

○Minghui Zhao<sup>1</sup>, Nozomi Kawamoto<sup>1</sup>, Kenji Kamiya<sup>1</sup>,  
Eika W. Qian<sup>1</sup> (1. Tokyo University of Agriculture and  
Technology)

10:30 AM - 10:45 AM

[2F07] [Invited] Oxidative coupling of methane over  
alkaline tungstate catalysts

○Kazuhiro Takanabe<sup>1</sup> (1. The University of Tokyo)

10:45 AM - 11:15 AM

Interenational sess.

## [1F07] Interenational sess. (1)

Chair:Shinya Furukawa(Hokkaido Univ.)

Thu. Oct 27, 2022 1:00 PM - 1:30 PM Room-F (13A Conf. room)

---

## [1F07] [Invited] Nano-metal phosphides as green sustainable hydrogenation catalysts

○Takato Mitsudome<sup>1,2</sup> (1. Osaka University, 2. PRESTO)

1:00 PM - 1:30 PM

# Nano-metal Phosphides as Green Sustainable Hydrogenation Catalysts

(Osaka University, PRESTO) Takato Mitsudome

## 1. Introduction

Currently available earth-abundant metal-based catalysts such as Raney catalysts are often employed for hydrogenation reactions and are effective. However, they face major drawbacks of being pyrophoric and unstable in air. Owing to these disadvantages, it is extremely difficult to handle them. Furthermore, they require severe reaction conditions, i.e., high H<sub>2</sub> pressure and high temperature due to their low activities. Focusing on these problems, we recently developed air-stable metal phosphide nanoparticle catalysts for the liquid-phase hydrogenation reactions.<sup>1,2</sup> The high performance of these catalysts will be presented.

## 2. Experiments

Well-defined cobalt and nickel phosphide nanoparticles (nano-Co<sub>2</sub>P and nano-Ni<sub>2</sub>P) were prepared by solvothermal method. Hydrogenation reactions were carried out in a 50 mL stainless steel autoclave equipped with a Teflon® vessel. Conversion and yield were determined by GC-MS analysis using an internal standard method.

## 3. Results and Discussion

The developed nano-Co<sub>2</sub>P is nanocrystal with a rod-like hexagonal prismatic structure with a length of 20 nm and a diameter of approximately 10 nm (Figure 1).<sup>1</sup> nano-Co<sub>2</sub>P can serve as a new class of catalyst for the hydrogenation of nitriles to the corresponding amines. nano-Co<sub>2</sub>P exhibits air stability and high activity for the nitrile hydrogenation with an excellent turnover number exceeding 49,000, which is over 20- to 500-fold greater than those previously reported. nano-Co<sub>2</sub>P also shows a broad substrate scope: a wide range of nitriles including di- and tetra-nitriles, were hydrogenated to primary amines even under just 1 bar of H<sub>2</sub> pressure, far milder than the conventional reaction conditions (Figure 2). This work is the first demonstration of metal phosphides capable of hydrogenation of carboxylic acid derivatives. We also succeeded in synthesizing a novel nickel phosphide nanoparticle (nano-Ni<sub>2</sub>P) and demonstrated its versatile use for the selective hydrogenation of different polar groups such as aldehydes, ketones, nitroarenes, and nitriles in water.<sup>2</sup> Especially, hydrotalcite-supported nano-Ni<sub>2</sub>P is applicable to the hydrogenation of sugar aldehydes such as D-glucose, D-xylose, and maltose in water under ambient pressure of H<sub>2</sub>, giving the corresponding D-sorbitol, D-xylitol, and maltitol, respectively in excellent yields. These catalysts can be recovered from the reaction mixture by simple filtration and are reusable with high catalytic activity. Detailed characterizations using XAFS, XPS, FT-IR, TEM and theoretical calculation reveal that the high performances of these metal phosphides are attributed to their metallic nature and increase of the *d*-electron density of metals near the Fermi level.

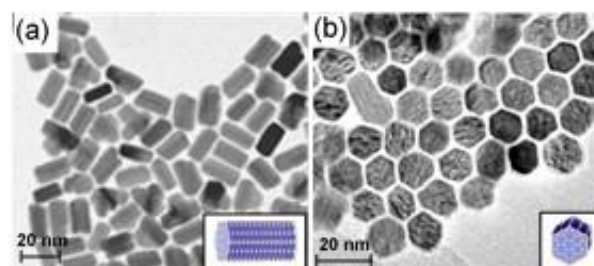


**Figure 1** TEM image of nano-Co<sub>2</sub>P from (a) side view and from (b) top view.

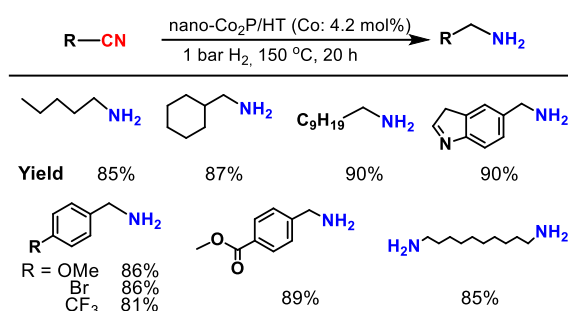


**Figure 2** Hydrogenation of nitriles using nano-Co<sub>2</sub>P catalyst under ambient pressure of H<sub>2</sub>.

## 4. Conclusion

Conclusively, such a metal phosphidation can provide a promising way to the design of advanced catalysts with high activity and stability for highly efficient and environmentally benign hydrogenation reactions.

## References

- 1) T. Mitsudome, M. Sheng, A. Nakata, J. Yamasaki, T. Mizugaki, K. Jitsukawa, *Chem. Sci.*, **2020**, 11 6682; H. Ishikawa, M. Sheng, A. Nakata, K. Nakajima, S. Yamazoe, J. Yamasaki, S. Yamaguchi, T. Mizugaki, T. Mitsudome, *ACS Catal.*, **2021**, 11, 750; M. Sheng, S. Fujita, S. Yamaguchi, J. Yamasaki, K. Nakajima, S. Yamazoe, T. Mizugaki, T. Mitsudome, *JACS Au*, **2021**, 1, 501; M. Sheng, S. Yamaguchi, A. Nakata, S. Yamazoe, K. Nakajima, J. Yamasaki, T. Mizugaki, T. Mitsudome, *ACS Sustain. Chem. Eng.*, **2021**, 9, 11238; H. Ishikawa, S. Yamaguchi, A. Nakata, K. Nakajima, S. Yamazoe, J. Yamasaki, T. Mizugaki, T. Mitsudome, *JACS Au*, **2022**, 2, 419.
- 2) S. Fujita, S. Yamaguchi, J. Yamasaki, K. Nakajima, S. Yamazoe, T. Mizugaki, T. Mitsudome, *Chem. Eur. J.*, **2021**, 27, 4439; S. Fujita, K. Imagawa, S. Yamaguchi, J. Yamasaki, S. Yamazoe, T. Mizugaki, T. Mitsudome, *Sci. Rep.*, **2021**, 11, 10673; S. Fujita, K. Nakajima, J. Yamasaki, T. Mizugaki, K. Jitsukawa, T. Mitsudome, *ACS Catal.*, **2020**, 10, 4261; S. Yamaguchi, S. Fujita, K. Nakajima, S. Yamazoe, J. Yamasaki, T. Mizugaki, T. Mitsudome, *Green Chem.*, **2021**, 23, 2010; S. Yamaguchi, S. Fujita, K. Nakajima, S. Yamazoe, J. Yamasaki, T. Mizugaki, T. Mitsudome, *ACS Sustain. Chem. Eng.*, **2021**, 9, 6347; S. Yamaguchi, T. Mizugaki, T. Mitsudome, *Eur. J. Inorg. Chem.*, **2021**, 2021, 3227.

International sess.

## [1F08-1F11] International sess. (2)

Chair:Shun Nishimura(National Inst. of Advanced Industrial Science &Technology)

Thu. Oct 27, 2022 1:30 PM - 2:30 PM Room-F (13A Conf. room)

---

### [1F08] Protection strategy for selective oxidative esterification of HMF-dimethylacetal to dimethylfuran-2,5-dicarboxylate with Au/CeO<sub>2</sub>

○Nirupama Sheet<sup>1</sup>, Jan J. Wiesfeld<sup>1</sup>, Atsushi Fukuoka<sup>1</sup>, Kiyotaka Nakajima<sup>1</sup> (1. Institute for Catalysis, Hokkaido University)

1:30 PM - 1:45 PM

### [1F09] Stereospecific ring opening metathesis polymerization of cyclic olefins by vanadium-alkylidene catalysts containing N-heterocyclic carbene ligands

○Jirapa Suthala<sup>1</sup>, Kotohiro Nomura<sup>1</sup> (1. Tokyo Metropolitan University)

1:45 PM - 2:00 PM

### [1F10] Synthesis of bio-based network polymers by acyclic diene metathesis polymerization

○Lance O'Hari P. Go<sup>1</sup>, Kotohiro Nomura<sup>1</sup> (1. Tokyo Metropolitan University)

2:00 PM - 2:15 PM

### [1F11] Conversion of *N*-acetylglucosamine derived from marine biomass chitin over ion-exchanged montmorillonite

○Kiyoyuki Yamazaki<sup>1</sup>, Norihito Hiyoshi<sup>1</sup>, Aritomo Yamaguchi<sup>1</sup> (1. The National Institute of Advanced Industrial Science and Technology(AIST))

2:15 PM - 2:30 PM

## Protection strategy for selective oxidative esterification of HMF-dimethylacetal to dimethylfuran-2,5-dicarboxylate with Au/CeO<sub>2</sub>

(Institute for Catalysis, Hokkaido University\*) ○Nirupama Sheet\*, Jan J. Wiesfeld\*, Atsushi Fukuoka\*, Kiyotaka Nakajima\*

### 1. Introduction:

The conversion of non-edible biomass resources into useful commodity chemicals is of great importance to build up a sustainable society.<sup>1</sup> 5-Hydroxymethylfurfural (HMF) is one of the versatile platform chemicals, which can be obtained from lignocellulosic biomass and can be converted into various value-added compounds including building blocks of advanced bio-based polymers. However, HMF reactions accompany severe and complex side reactions to produce insoluble polymerized species, so-called humins and these side reactions are predominant in concentrated solutions. Protection of the reactive formyl group as its acetal with 1,3-propanediol (PDO) enabled the use of concentrated solutions (10–20 wt%) in various redox reactions and ensured high productivity of the intended products.<sup>2–4</sup> In this study, we applied dimethylacetal protected HMF (OMe-HMF) in the oxidative esterification with a CeO<sub>2</sub>-supported Au catalyst for stepwise synthesis of dimethylfuran-2,5-dicarboxylate (MFDC), aiming at a cost-effective, highly selective, and productive process.

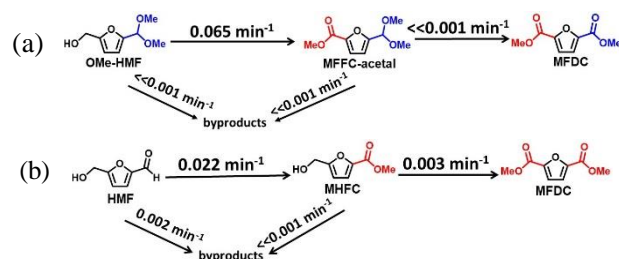
### 2. Experiment:

OMe-HMF was prepared by the acetalization of HMF with methanol. A ceria supported gold catalyst (Au/CeO<sub>2</sub>) was synthesized by deposition-precipitation method.<sup>3</sup> Oxidative esterification of HMF and OMe-HMF was conducted in pressure resistant Teflon-lined stainless steel autoclave reactors. A mixture of substrate (HMF or OMe-HMF, 100 mg), Au/CeO<sub>2</sub> (100 mg), and Na<sub>2</sub>CO<sub>3</sub> (1 mol%) in methanol (1 g, 10 wt%) was stirred under pressurized oxygen (0.9 MPa) at 373 K for specific time. After reaction, the reaction mixture was diluted with ethyl acetate (50 mL) to dissolve all products and analyzed with GC (Shimadzu, GC-2014) using chlorobenzene as an internal standard.

### 3. Results and Discussion:

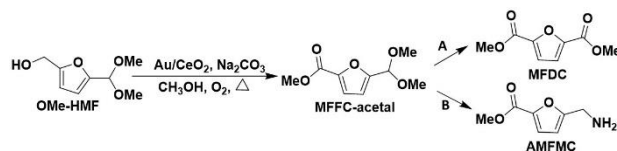
Oxidative esterification of OMe-HMF exclusively produces dimethylacetal form of methyl-5-formylfuran-2-carboxylate (MFFC-acetal) in a 96% yield with a satisfactory value of carbon balance (97%) when the reaction was performed at 373 K for 2 h. In contrast, oxidative esterification of HMF gave the mixtures of methyl-5-(hydroxymethyl)furan-2-carboxylate (MHFC),

MFDC, and other byproducts under the same reaction conditions.



**Scheme 1.** Kinetics studies on oxidative esterification of (a) OMe-HMF acetal (10 wt%) and (b) HMF (10 wt%) in methanol with Au/CeO<sub>2</sub>

The difference between HMF and OMe-HMF was further confirmed by kinetic studies using 10 wt% solutions (Scheme 1). Oxidative esterification of -CH<sub>2</sub>OH in OMe-HMF proceeds faster as evidenced by a large rate constant (0.065 min<sup>-1</sup>). Small rate constants ( $\ll 0.001 \text{ min}^{-1}$ ) in the formation of byproducts and MFDC suggest that dimethylacetal group is stable against both oxidative esterification and side reactions to form MFDC and byproducts, respectively. MFFC-acetal can be used as an intermediate to synthesize MFDC selectively with additional reaction steps. Moreover, high MFFC-acetal yields were obtained after the increase in OMe-HMF concentration (95% for 15 wt% and 90% for 20 wt%) under the same conditions. MFFC-acetal can also be used to synthesize several other bio-based monomers such as 5-aminomethylfuran-2-methyl carboxylate (AMFMC) through reductive amination (Scheme 2).



**Scheme 2.** Reaction network from OMe-HMF to MFDC and AMFMC via MFFC-acetal

1) Jin, M. et al., *Catal. Today*, 2021, 367, 2–8. 2) Kim, M. et al., *Angew. Chem. Int. Ed.*, 2018, 57, 8235–8239. 3) Kim, M. et al., *ACS Catal.*, 2019, 9, 4277–4285. 4) Wiesfeld, J. J. et al., *Green Chem.*, 2020, 22, 1229–1238.

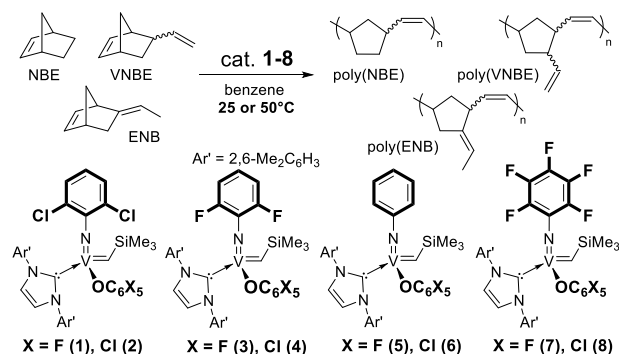
# Stereospecific ring opening metathesis polymerization of cyclic olefins by vanadium–alkylidene catalysts containing *N*-heterocyclic carbene ligands

(都立大院理) ○Jirapa Suthala, and Kotohiro Nomura\*

## 1. Introduction

(Arylimido)vanadium(V) alkylidene complexes containing anionic donor ligands have been known to exhibit from moderate to high catalytic activities in the ring opening metathesis polymerization (ROMP) of cyclic olefins;<sup>1-3</sup> certain catalysts show the high *Z*-selectivity and the ligand modification plays a key role.<sup>2</sup> *N*-Heterocyclic carbene (NHC) ligands are known to stabilize high oxidation state organometallic complexes with early transition metals.<sup>4,5</sup>

Herein, we present the synthesis of a series of (arylimido)vanadium(V) alkylidene NHC complexes containing halogenated phenoxy ligands and their use as catalysts for ROMP of norbornene (NBE) and the derivatives including the ligand effect toward the catalytic activity, *cis* specificity and the tacticity control (Scheme 1).<sup>6</sup>



## 2. Experimental

All experiments were carried out under nitrogen atmosphere using standard Schlenk techniques or using a Vacuum Atmosphere Drybox. Molecular weights and molecular weight distributions of the resultant polymers were analyzed by GPC in THF vs polystyrene standards, and structures of the polymer were analyzed by NMR spectra.

## 3. Results and discussion

The phenoxy alkylidene complexes, V(CHSiMe<sub>3</sub>)-(NAr')(OC<sub>6</sub>X<sub>5</sub>)(NHC) (**1-8**), were prepared from the dialkyl complexes by treating with the NHC through

$\alpha$ -hydrogen elimination. The catalysts were identified by NMR spectra and elemental analysis.

Selected results in the ROMP of NBE using complexes **1-8** are summarized in Table 1. Complexes **1**, **2** and **8** at 25°C afforded ring opened poly(NBE)s with high molecular weight ( $M_n = 956,000$ ), with high *Z*-selectivity (98 %) as well as with high *syndiotactic* stereoregularity; the turnover frequencies (TOFs) reached 905,000 h<sup>-1</sup> (251 sec<sup>-1</sup>) by **7**. In contrast, the phenylimido analogues (**5,6**) afforded atactic polymers containing a mixture of *cis/trans* olefinic double bonds. We wish to report our explored results including the living polymerization and the *cis*-syndiospecific ROMPs of NBE derivatives in the symposium.

Table 1. ROMP of NBE by using **1-3**<sup>a</sup>

cat.	yield	TOF <sup>b</sup>	$M_n^c$	$M_w/M_n^c$	<i>cis</i> <sup>d</sup>
/ $\mu\text{mol}$	/ %	/ h <sup>-1</sup> (s <sup>-1</sup> )	$\times 10^{-4}$	$M_n^c$	/ %
<b>1</b> (0.1)	59	750000 (208)	77.8	2.65	94
<b>1</b> <sup>e</sup> (0.1)	90	573000 (158)	<b>95.6</b>	2.69	94
<b>2</b> (0.1)	42	530000 (147)	56.6	2.16	<b>98</b>
<b>3</b> (0.1)	62	790000 (219)	81.9	2.80	69
<b>4</b> (0.1)	56	714000 (198)	59.4	2.06	82
<b>5</b> (0.3)	85	361000 (100)	58.7	2.14	50
<b>6</b> (0.3)	51	215000 (59.6)	44.0	1.97	64
<b>7</b> (0.1)	71	<b>905000 (251)</b>	60.6	2.20	75
<b>8</b> (0.1)	58	739000 (205)	70.4	2.21	87

<sup>a</sup>Conditions: NBE 200 mg (2.12 mmol), benzene 4.8 mL (initial NBE conc. 0.44 mmol/mL). <sup>b</sup>TOF = TON/time. <sup>c</sup>GPC data in THF vs polystyrene standards. <sup>d</sup>*Cis* percentage (%) estimated by <sup>1</sup>H NMR spectra. <sup>e</sup>Reaction time is 2 minutes.

## References

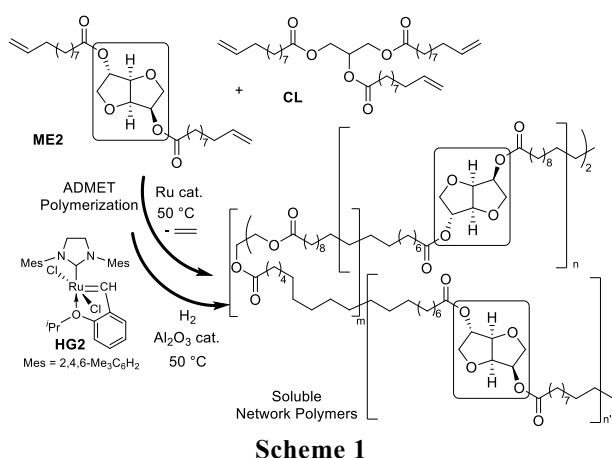
- Nomura, K.; Hou, X. *Dalton Trans.* **2017**, *46*, 12.
- Hou, X.; Nomura, K. *J. Am. Chem. Soc.* **2015**, *137*, 4662; **2016**, *138*, 11840.
- Chaimongkolkunasin, S.; Nomura, K. *Organometallics* **2018**, *37*, 2064.
- Zhang, W.; Nomura, K. *Organometallics* **2008**, *27*, 6400.
- Buchmeiser, M. R. *Chem. Eur. J.* **2018**, *24*, 14295.
- Kawamoto, Y.; Elser, I.; Buchmeiser, M. R.; Nomura, K. *Organometallics* **2021**, *40*, 2017.

# Synthesis of bio-based network polymers by acyclic diene metathesis polymerization

(都立大院理) ○Lance O'Hari P. Go, and Kotohiro Nomura\*

## 1. Introduction

Synthesis of recyclable polymers from renewable feedstocks, resulting in mechanically tough product, is of interest for solving the “plastic waste” concerns.<sup>1</sup> One alternative to fossil polymers are bio-based polyesters, which can be sourced from bio-renewable feedstocks and are converted to monomers or fine chemicals via ester bond cleavage. This work demonstrates synthesis of novel type of bio-sourced network polyesters, made from an isosorbide-based diene monomer (**ME2**) and a glycerol-based crosslinker (**CL**), polymerized via ADMET polymerization followed by tandem hydrogenation to make a tough soluble network polyester (**Scheme 1**).



## 2. Experimental

All experiments were carried out under a nitrogen atmosphere. One step approach was performed by mixing **ME2** and **CL** at the beginning while the two-step approach required pre-polymerization of **ME2** before addition of **CL**.<sup>2</sup> Saturated polyesters were obtained by the tandem hydrogenation from the ADMET reaction mixture upon addition of  $\text{Al}_2\text{O}_3$ .<sup>3</sup> Molecular weights ( $M_n$ ) and molecular weight distributions ( $M_w/M_n$ ) of the resultant polymers were analyzed by GPC, thermal properties by DSC, and mechanical properties by a compact tensile tester.

## 3. Results and discussion

Selected results in the network polymer synthesis are summarized in **Table 1**. The  $M_n$  values in the soluble network polymer were affected by amount of

**CL** used. The  $M_n$  values of the polymer by using 5.0 mol % of **CL** were less than 20,000, whereas a lower **CL** (2.5 and 1.0 mol %) resulted in the polymers with higher  $M_n$  values (30,000 and 37,000, respectively). The resultant polymers going above these thresholds became gel with large PDI ( $M_w/M_n$ ) values.

Mechanical analysis shows that the soluble network polymers prepared by 5.0 mol % **CL** showed higher max strain (elongation at break) with slight decrease in the ultimate strength compared to the linear polymer without **CL** of same  $M_n$  value. In addition, using lower concentrations of **CL** yielded the network polymers with higher  $M_n$  values, thereby resulting in significant increase in ultimate strength and max strain (**Table 1**, row 7). These results also suggest that a two-step synthesis approach showed better mechanical properties compared to one-step synthesis approach.

**Table 1.** Synthesis of network polymers by ADMET polymerization of **ME2** in the presence of **CL** (1-step or two-step synthesis approach).

CL mol % (approach)	$M_n^b$ $\times 10^{-4}$	$M_w/M_n^b$	strength <sup>c</sup> N/mm <sup>2</sup> ( $\pm$ )	max strain <sup>c</sup> % ( $\pm$ )
5.0 (1-step)	1.64	5.45 <sup>d</sup>	7.2 ( $\pm 0.2$ )	173 ( $\pm 9$ )
none	2.18	1.77	11.0 ( $\pm 0.7$ )	31.4 ( $\pm 18$ )
2.5 (1-step)	2.59	2.90	13.0 ( $\pm 0.8$ )	251 ( $\pm 32$ )
2.5 (2-step)	2.55	4.95 <sup>d</sup>	14.0 ( $\pm 0.5$ )	335 ( $\pm 19$ )
none	2.79	1.98	9.0 ( $\pm 0.3$ )	193 ( $\pm 5$ )
1.0 (1-step)	3.66	2.45	13.8 ( $\pm 4.3$ )	243 ( $\pm 26$ )
1.0 (2-step)	3.68	2.92	23.0 ( $\pm 5.9$ )	534 ( $\pm 100$ )
none	4.30	1.88	21.2 ( $\pm 1.9$ )	373 ( $\pm 27$ )

<sup>a</sup>Conditions: monomer **ME2** 900 mg (2.0M), 2 mol % **HG2** catalyst, 50 °C. <sup>b</sup>GPC data in THF vs. polystyrene standards. <sup>c</sup>Stress-strain curves measured at a rate of 10 mm/min at 23 °C. <sup>d</sup>Onset of Gel formation.

## References

- (1) K. Nomura, N. W. B. Awang, *ACS Sustainable Chem. Eng.*, 2021, **9**, 5486-5505.
- (2) D. Le, C. Samart, S. Kongparakul, K. Nomura. *RSC Adv.*, 2019, **9**, 10245-10252.
- (3) K. Nomura, P. Chaijaroen, M.M. Abdellatif. *ACS Omega*, 2020, **5**, 18301-18312.

## Conversion of *N*-acetylglucosamine derived from marine biomass chitin over ion-exchanged montmorillonite

(AIST) ○Kiyoyuki Yamazaki・Norihito Hiyoshi・Aritomo Yamaguchi

### 1. Introduction

Chitin is marine biomass and contained in crustacean. *N*-acetylglucosamine (NAG), which is a monomer of chitin, can be feedstock of various valuable nitrogen-containing chemicals. 3-acetylamino-5-acetylfuran (3A5AF), which is one of products of NAG conversion, is a prospective platform for pharmaceuticals such as anti-cancer agent<sup>1</sup> and pesticides<sup>2</sup>.

Conversion of NAG to 3A5AF (Fig.1) could be catalyzed by various homogeneous catalysts<sup>3-4</sup> such as metal chlorides, boric acid, and ionic liquids. However, these catalysts were used excessively over the NAG amount and required to be separated from products. Therefore, in this study, we considered solid acid catalysts such as ion-exchanged montmorillonite to reduce the separation cost.

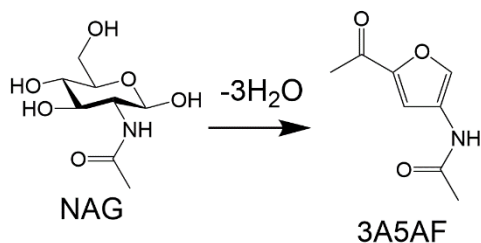


Fig.1 NAG conversion to 3A5AF

### 2. Experimental

Ion-exchanged montmorillonite was prepared as follows. Na<sup>+</sup> containing montmorillonite (Kunipia-F, Na<sup>+</sup>mont) 20 g, Al nitrate nonahydrate 30 g, and water 160 g were added into an eggplant flask and stirred for 2 h. Then, the solution was filtered. After washing by ethanol aqueous solution, dried residue was crushed by ball mill and ion-exchanged montmorillonite (Al-Na<sup>+</sup>mont) was obtained.

NAG conversion was carried out in a batch reactor. NAG 6.8 mmol, solid acid catalyst 2.0 g, dimethyl acetamide 30 mL, and NaCl 2.0 mmol were put into the reactor (100 cm<sup>3</sup>). Then, the reactor was heated

at 433 K for 2 h. Products were quantified by high performance liquid chromatography.

### 3. Results and Discussion

Table 1 shows product yields of NAG conversion over solid catalysts such as Na<sup>+</sup>mont, Al-Na<sup>+</sup>mont, K-10 (H<sup>+</sup> containing montmorillonite), MFI-type zeolite (SiO<sub>2</sub>/Al<sub>2</sub>O<sub>3</sub>=40), Amberlyst15 (cation exchange resin), SiO<sub>2</sub> · MgO. Al-Na<sup>+</sup>mont, K-10, MFI, Amberlyst15 was found to be active for 3A5AF formation and Al-Na<sup>+</sup>mont was the best among the applied catalysts. These facts indicate that dehydration of NAG to 3A5AF would be catalyzed by acid. Though, solid acid such as Al-Na<sup>+</sup>mont, K-10, and MFI would also catalyze deacetylation and lead up to form 5-hydroxymethyl furfural (HMF). To improve 3A5AF yield, modification of acidity to catalyze dehydration and suppress deacetylation would be needed.

Table 1. Yields of products in NAG conversion

Solid catalysts	NAG conversion / %	3A5AF yield / %	HMF yield / %
1 None	93	0.9	0.0
2 Na <sup>+</sup> mont	97	0.0	0.0
3 Al-Na <sup>+</sup> mont	99	14	15
4 K-10	96	8.2	9.0
5 MFI	83	8.6	18
6 Amberlyst15	100	8.1	0.0
7 SiO <sub>2</sub> · MgO	97	1.3	0.0

1. A. D. Sadiq, et al., *ChemSusChem*, **2018**, 11, 532.
2. T.T. Pham, et al., *Green Chem.* **2020**, 22 (6), 1978.
3. K. W. Omari, et al., *ChemSusChem*, **2012**, 5, 1767.
4. J. Wang, et al., *J., Sci. Total Environ.*, **2020**, 710, 7.

International sess.

## [1F12-1F14] International sess. (3)

Chair: Yasutaka Kuwahara (Osaka Univ.)

Thu. Oct 27, 2022 2:45 PM - 3:45 PM Room-F (13A Conf. room)

---

### [1F12] [Invited] Low-dimensional assembling of iron-aqua complexes for designing post-TiO<sub>2</sub>

○Yusuke Ide<sup>1</sup> (1. National Institute for Materials Science, International Center for Materials Nanoarchitectonics)

2:45 PM - 3:15 PM

### [1F13] Development of thermally stable highly dispersed supported polyoxometalate cesium salts

○Takaaki Suzuki<sup>1</sup>, Tomohiro Yabe<sup>1</sup>, Keiju Wachi<sup>1</sup>, Kentaro Yonesato<sup>1</sup>, Kosuke Suzuki<sup>1</sup>, Kazuya Yamaguchi<sup>1</sup> (1. the University of Tokyo)

3:15 PM - 3:30 PM

### [1F14] Crystalline Zr<sub>3</sub>SO<sub>9</sub> oxides with superior acid catalytic property to the conventional sulfated zirconia

○Meilin Tao<sup>1</sup>, Satoshi Ishikawa<sup>1</sup>, Takuji Ikeda<sup>2</sup>, Shunsaku Yasumura<sup>3</sup>, Yuan Jing<sup>3</sup>, Takashi Toyao<sup>3</sup>, Ken-ichi Shimizu<sup>3</sup>, Hiromi Matsuhashi<sup>4</sup>, Wataru Ueda<sup>1</sup> (1. Kanagawa University, 2. Research Institute for Chemical Process Technology, National Institute of Advanced Industrial Science and Technology (AIST), 3. Institute for Catalysis, Hokkaido University, 4. Hokkaido University of Education)

3:30 PM - 3:45 PM

## Low-dimensional assembling of iron-aqua complexes for designing post-TiO<sub>2</sub>

(National Institute for Materials Science) Yusuke Ide

TiO<sub>2</sub> nanoparticles are widely used in sunscreens, cosmetics, photocatalysts, and so on. However, the use of these nanoparticles raises health concerns; for instance, their nanometric size/nanoscale reactivities can lead to cytotoxicity. Because TiO<sub>2</sub> nanoparticles are released into the environment during their manufacturing and subsequent use, humans will increasingly be exposed to TiO<sub>2</sub> nanoparticles, which can enter the body via the skin and inhalation. The classification of TiO<sub>2</sub> as a category-2 carcinogen by the European Commission has motivated us to develop suitable materials (e.g., photocatalyst, UV absorbers as active ingredients in sunscreen products) to replace TiO<sub>2</sub> nanoparticles.

In terms of abundance and environmental compatibility, Fe and Fe oxides (as well as Fe oxyhydroxides) are good candidates for post-TiO<sub>2</sub> materials. However, typical Fe-oxide crystals like hematite are not white, unlike TiO<sub>2</sub>, because they absorb visible light (to near-infrared light). Also, typical Fe-oxide crystals show a poor photocatalytic activity considerably lower than that of TiO<sub>2</sub> nanoparticles. In contrast, aqua-Fe(III) complexes (e.g. [Fe<sup>III</sup>(H<sub>2</sub>O)<sub>6</sub>]<sup>3+</sup>) and their dimers (e.g. [(H<sub>2</sub>O)<sub>4</sub>Fe<sup>III</sup>(OH)<sub>2</sub>Fe<sup>III</sup>(H<sub>2</sub>O)<sub>4</sub>]<sup>4+</sup>) have wider energy gaps (band gaps) than Fe-oxide crystals; thus absorb UV light, and show a good photocatalytic activity comparable to TiO<sub>2</sub> nanoparticles. However, these

aqua-Fe(III) complexes are extremely unstable because [Fe<sup>III</sup>(H<sub>2</sub>O)<sub>6</sub>]<sup>3+</sup> is stable only in strongly acidic solutions (pH < 0.2) and undergoes rapid hydrolysis and condensation to form colored Fe-oxide clusters and crystals when the solution pH increases.

Despite the ubiquity of aqua-Fe(III) complexes in biological enzymes (Fig. 1A) and their useful properties and cost-effectiveness for many applications, artificially stabilising these fleeting molecules for practical use remains challenging in terms of their stability, the precise control of aqua-Fe(III) complex structures, and the safety of supports. Herein, we demonstrate that dimeric aqua-Fe(III) species can be stabilised using mesoporous silicas and layered silicates (Fig. 2B) to produce photocatalysts and UV absorbers, respectively, whose performances exceed to that of commercial TiO<sub>2</sub> nanoparticles.<sup>1,2</sup> We also report that an exceptional type of green rust, which is a Fe(II)/Fe(III) mixed-valent iron mineral and previously thought to be very instable against oxidation, shows high oxidation stability and good photocatalytic activity higher than that of a benchmark TiO<sub>2</sub> nanoparticle.<sup>3</sup>

### References

1. Y. Ide et al., *Chem. Sci.* 2019, 10, 6604.
2. H. El-Hosainy et al., *Mater. Today Nano* 2022, 19, 100227.
3. R. Tahawy et al., *Appl. Catal. B* 2021, 286, 119854.

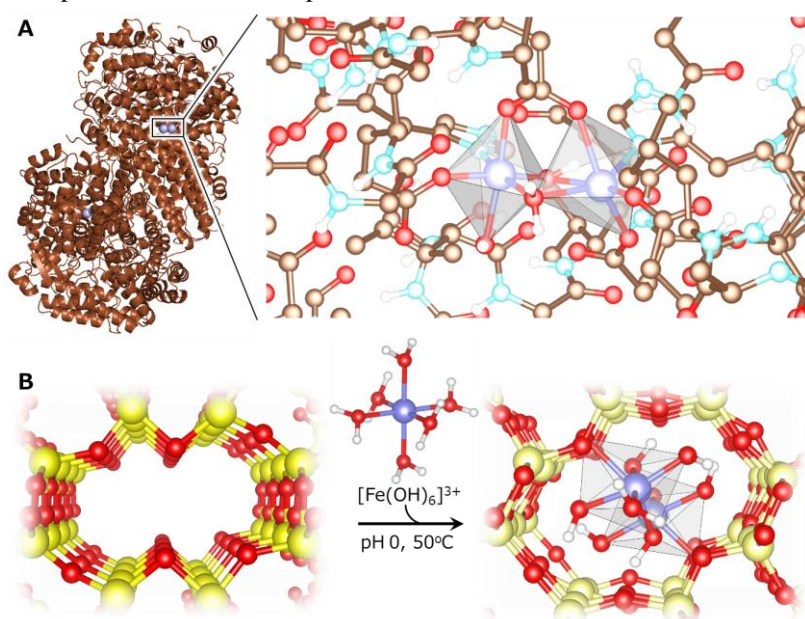


**Fig. 1.** Dimeric aqua-Fe(III) species in a natural enzyme and the present material. (A) Dimeric Fe(III) active site, represented by grey octahedra, in methane monooxygenase hydroxylase enzyme (Protein Data Bank accession code, 1MTY). (B) Schematic representation for the stabilisation of a dimeric aqua-Fe(III) species within a microporous layered silicate.

## Development of thermally stable highly dispersed supported polyoxometalate cesium salts

(The University of Tokyo) ○Takaaki Suzuki, Tomohiro Yabe, Keiju Wachi, Kentaro Yonesato, Kosuke Suzuki, Kazuya Yamaguchi

### 1. Introduction

Polyoxometalates (POMs) are anionic metal–oxo clusters typically consisting of metal–oxygen polyhedral units. We recently formed various POM tetra-*n*-butylammonium (TBA) salts with well-defined multinuclear structures.<sup>1)</sup> Generally, to increase the effective surface area, POMs are utilized as heterogeneous catalysts including supported POMs. However, POM TBA salts are easily decomposed under high-temperature conditions thus might be unsuitable for aerobic oxidation.

In this study, we developed a new cation-exchange method from supported-POM TBA salts to supported-POM Cs salts in organic solvents in order to provide thermal stability and effective surface area to POMs.

### 2. Experimental

TBA<sub>4</sub>PVMo<sub>11</sub>O<sub>40</sub> (TBA-PVMo11), synthesized as previously reported,<sup>2)</sup> was dispersed on various supports such as Al<sub>2</sub>O<sub>3</sub> using the incipient wetness method (named TBA-PVMo11/Al<sub>2</sub>O<sub>3</sub>). TBA-PVMo11/Al<sub>2</sub>O<sub>3</sub> was dispersed in a solution containing a Cs source. After stirring the dispersion for 2 h, the precipitate was filtered, washed, and collected (named Cs-PVMo11/Al<sub>2</sub>O<sub>3</sub>).

### 3. Results and Discussion

20 wt% TBA-PVMo11/Al<sub>2</sub>O<sub>3</sub> was prepared and <sup>51</sup>V and <sup>31</sup>P MAS NMR spectra confirmed the same chemical environments of V<sup>5+</sup> and P<sup>5+</sup> in TBA-PVMo11 and TBA-PVMo11/Al<sub>2</sub>O<sub>3</sub> (Figure 1). Then, the preparation of Cs-PVMo11/Al<sub>2</sub>O<sub>3</sub> via cation exchange from TBA-PVMo11 to Cs-PVMo11 on Al<sub>2</sub>O<sub>3</sub> was investigated. When cesium

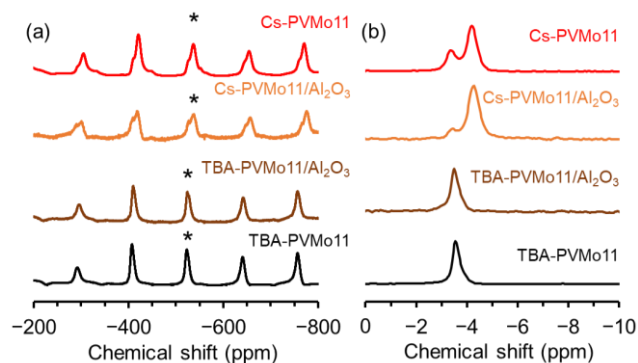


Figure 1. (a) <sup>51</sup>V and (b) <sup>31</sup>P MAS NMR spectra.

trifluoromethanesulfonate (CsOTf) was used in ethanol, the cation exchange completely proceeded and the chemical environment around V<sup>5+</sup> and P<sup>5+</sup> of Cs-PVMo11/Al<sub>2</sub>O<sub>3</sub> was supposed to be similar to that of the as-prepared Cs-PVMo11 (Figure 1). The cation exchange using CsOTf in ethanol had the wide support applicability.

Mo K-edge XANES was performed to investigate the coordination states of Mo atoms in Cs-PVMo11/Al<sub>2</sub>O<sub>3</sub>, and the pre-edge peak of the Mo K-edge XANES spectrum of Cs-PVMo11/Al<sub>2</sub>O<sub>3</sub> slightly differed from that of Cs-PVMo11 (Figures 2a,b); the octahedral {MoO<sub>6</sub>} units in Cs-PVMo11/Al<sub>2</sub>O<sub>3</sub> were presumed to be distorted on the Al<sub>2</sub>O<sub>3</sub> support possibly due to the strong interaction. In fact, HAADF-STEM indicated that Cs-PVMo11 was highly dispersed on Al<sub>2</sub>O<sub>3</sub> (Figures 2c,d). Notably, Cs-PVMo11/Al<sub>2</sub>O<sub>3</sub> showed favorable thermal stability against the calcination at 573 K for 3 h under an O<sub>2</sub> atmosphere.

In conclusion, a new cation-exchange method using CsOTf in ethanol was developed to obtain thermally stable highly dispersed supported POM Cs salts from the corresponding TBA salts on supports.

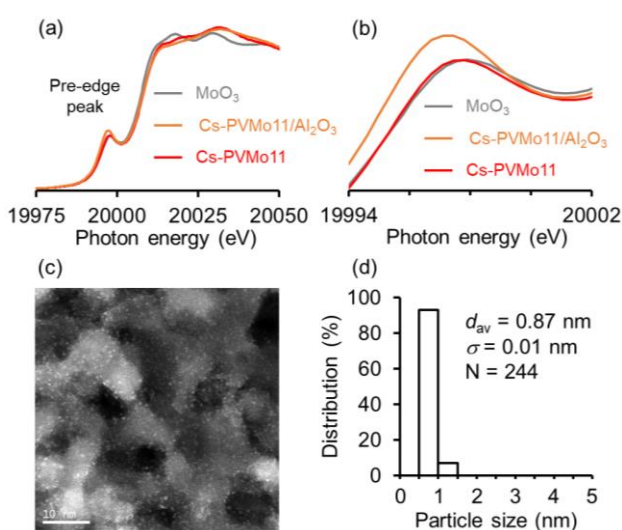


Figure 2. (a) Mo K-edge XANES spectra and (b) a magnification of the pre-edge region. (c) A HAADF-STEM image and (d) a histogram on the size distribution of Cs-PVMo11/Al<sub>2</sub>O<sub>3</sub>.

1) Y. Sunada *et al.*, *Coord. Chem. Rev.*, **469**, 214673 (2022).

2) K. Nomiya *et al.*, *J. Mol. Catal. A*, **126**, 43–53 (1997).

## Crystalline $Zr_3SO_9$ Oxides with Superior Acid Catalytic Property to the Conventional Sulfated Zirconia

(Kanagawa Univ.\* · AIST\*\* · Hokkaido Univ.\*\*\* · Hokkaido Univ. of Edu.\*\*\*\*) ○ TAO, Meilin\* · ISHIKAWA, Satoshi\* · IKEDA, Takuji \*\* · YASUMURA, Shunsaku\*\*\* · JING, Yuan\*\*\* · TOYAO, Takashi\*\*\* · SHIMIZU, Ken-ichi\*\*\* · MATSUHASHI, Hiromi\*\*\*\* · UEDA, Wataru\*

### 1. Introduction

Sulfated zirconia (SZ) has attracted extensive attention because of its strong acidity and high activity in numerous acid catalyzed reactions. Much work has been devoted to study the state of sulfur species on the surface of zirconium oxides. However, the precise structure model of this material is still under debate. Here, we successfully obtained a crystalline  $Zr_3SO_9$  material, and investigated its catalytic activity for acid reactions. The resulting material exhibited superior acid catalytic properties to the conventional sulfated zirconia (SZ). In addition, the catalytical active species of  $Zr_3SO_9$  were clarified based on the crystal structure.

### 2. Experimental

$Zr_3SO_9$  was obtained by hydrothermal synthesis (240 °C, 72 h) of  $ZrOCl_2$  in  $H_2SO_4$  solution (Zr concentration: 0.5 M). Sulfated zirconia (SZ) was prepared by a conventional method. Other catalysts used for comparison are obtained from Catalysis Society of Japan.

### 3. Results and Discussion

The initial crystal structure of  $Zr_3SO_9$  was obtained by *ab-initio* structural analysis (Fig. 1). It is a layered material with interstitial distance of 10.4 Å. In the cross-section of the material, Zr and O connected with each other to form a hexagonal-shaped texture. S species are located uniformly over the sheet in the state of sulfate anion ( $SO_4^{2-}$ ) as confirmed by IR measurements and DFT calculations. The crystal structure could be successfully refined by Rietveld method.

Isomerization of n-butane was carried out by pulse reactor over  $Zr_3SO_9$  and other typical solid acid catalysts including SZ (Fig. 2a). Compared with other typical acid catalysts,  $Zr_3SO_9$  exhibited superior catalytic activity for this reaction under the same conditions in the catalyst weight basis. The conversion of n-butane was three times higher than that of SZ in the catalyst weight basis and was nine times in the S amount basis. In addition, the catalytic activity of  $Zr_3SO_9$  was highly improved by the introduction of water. From the experiment results and DFT calculation, it was clarified that Zr anchoring  $SO_4^{2-}$

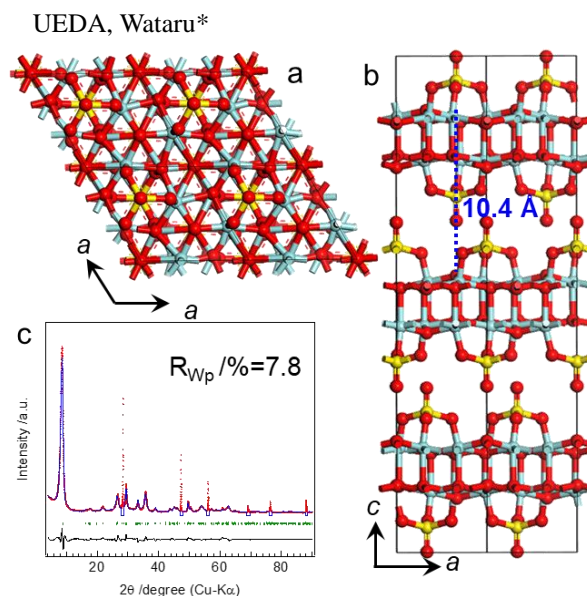


**Fig. 1.** (a) (b) Structure model of  $Zr_3SO_9$ ; (c) Rietveld refinement.

acts as the Lewis acid site, and water once introduced can coordinate to the Zr site, which leads to the transformation of Lewis acid site to Brønsted acid site. This might be the main reason why  $Zr_3SO_9$  exhibited a substantial catalytic activity. n-Butane isomerization was also carried out for  $Zr_3SO_9$  and SZ with Pt loading (3wt%) in the continuous flow conditions under a diluted hydrogen gas flow (Fig. 2b). The activity without Pt dropped significantly in both cases. 3wt%Pt/ $Zr_3SO_9$  shows superior activity than 3wt%Pt/SZ. The selectivity of i-butane was above 98%.

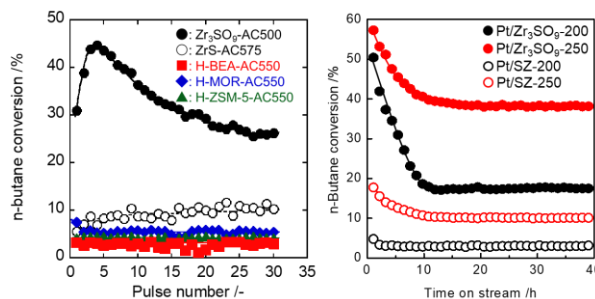


**Fig. 2.** (a) Isomerization of n-butane over  $Zr_3SO_9$  and typical acid catalysts by pulse at 300 °C. AC means calcination under air atmosphere. (b) Isomerization of n-butane over  $Zr_3SO_9$  and SZ with Pt loading (3 wt%) in the continuous flow conditions at 200 °C (black) and 250 °C (red).

International sess.

## [2F01-2F04] International sess. (4)

Chair: Naohiro Shimoda (Tokushima Univ.)

Fri. Oct 28, 2022 9:00 AM - 10:00 AM Room-F (13A Conf. room)

---

### [2F01] CeO<sub>2</sub>-supported bimetallic Ni-Ag catalyst for ammonia synthesis from NO-CO-H<sub>2</sub>O

Chandan Chaudhari<sup>1</sup>, Yuichi Manaka<sup>1,2</sup>, Tetsuya Nanba<sup>1</sup> (1. Fukushima Renewable Energy Institute, AIST, 2. School of Materials and Chemical Technology, Tokyo Institute of Technology)

9:00 AM - 9:15 AM

### [2F02] Plasmon-assisted hydrogenation and dehydrogenation reactions of noble metal nanoparticles

Priyanka Verma<sup>1</sup>, Kohsuke Mori<sup>2</sup>, Yasutaka Kuwahara<sup>2</sup>, Ryo Watanabe<sup>1</sup>, Hiromi Yamashita<sup>2</sup>, Choji Fukuhara<sup>1</sup> (1. Shizuoka University, 2. Osaka University)

9:15 AM - 9:30 AM

### [2F03] Effect of Ca addition on the catalytic activity of BaTiO<sub>3</sub> for oxidative coupling of methane

Rongguang Gan<sup>1</sup>, Yoshihide Nishida<sup>1</sup>, Massaki Haneda<sup>1</sup> (1. Nagoya Institute of Technology)

9:30 AM - 9:45 AM

### [2F04] CO<sub>2</sub> hydrogenation reaction over Pd-containing MWW zeolite catalyst

Willie Yang<sup>1</sup>, Shuhei Yasuda<sup>1</sup>, Sridharan Balu<sup>2</sup>, Muyuan Yu<sup>1</sup>, Toshiki Kaseguma<sup>1</sup>, Toshiyuki Yokoi<sup>1</sup> (1. Tokyo Institute of Technology, 2. National Taipei University of Technology)

9:45 AM - 10:00 AM

CeO<sub>2</sub> 担持 Ni-Ag 二元系触媒を用いた NO-CO-H<sub>2</sub>O 反応によるアンモニア合成

## CeO<sub>2</sub>-supported bimetallic Ni-Ag catalyst for ammonia synthesis from NO-CO-H<sub>2</sub>O

(AIST<sup>1</sup>, Tokyo Tech<sup>2</sup>) C. Chaudhari,<sup>1</sup> K. Kobayashi,<sup>1</sup> O.Y. Manaka,<sup>1,2\*</sup> T. Nanba<sup>1</sup>

### 1. Introduction

The emission of NO is cause of various environmental problems such as acid rain and photochemical smog. Therefore, it is necessary to reduce the concentration of NO. Ammonia can be prepared from NO (Nitrogen oxide To Ammonia: NTA) which is an attractive alternative for NO abatement. Our group developed Pt/TiO<sub>2</sub> catalyst for ammonia synthesis on NO-CO-H<sub>2</sub>O reaction.<sup>1</sup> However, the cost of Pt is a barrier for industrial applications. Recently, we developed Ni/CeO<sub>2</sub> catalyst for NTA reaction. Moderate yield (55%) of ammonia was obtained. In this study, we investigated the effect of second metal (M= Fe, Co, Cu, Ag) on the activity of Ni/CeO<sub>2</sub>.

### 2. Experimental

CeO<sub>2</sub> support was purchased from Daichi Kigenso company and calcined at 700 °C for 4 h. 10 wt% Monometallic Ni or Ag and bimetallic 10 wt % Ni<sub>x</sub>Ag<sub>1-x</sub> (x = 0.3, 0.5, 0.7) catalysts were prepared by an incipient wetness method with using different second metal. The catalysts were characterized by BET, XRD, H<sub>2</sub>-TPR and CO-adsorption. The catalytic activity was measured by a fixed-bed flow reactor. The feed gas was composed of 0.1 % NO, 0.3% CO and 1% H<sub>2</sub>O ppm with dilution by Ar. The total flow was set to 250 mL/min. The product gases were analyzed online Fourier transform infrared spectroscopy and gas chromatography.

### 3. Results and Discussion

Initially, we prepared 5Ni5Fe/CeO<sub>2</sub>, 5Ni5Co/CeO<sub>2</sub>, 5Ni5Cu/CeO<sub>2</sub> and 5Ni5Ag/CeO<sub>2</sub> catalysts and examined for NTA reaction. All catalysts showed full conversion (100%) of NO above 200 °C (Figure 1). 5Ni5Ag/CeO<sub>2</sub> showed high yield (62%) ammonia (Figure 2). Higher Ni or Ag concentration in NiAg/CeO<sub>2</sub> catalyst was not favorable for ammonia formation. The activity of monometallic (Ni or Ag) and bimetallic (NiAg) was compared. Ag/CeO<sub>2</sub> was unable to produce below 300 °C. Ni/CeO<sub>2</sub> gave 55% yield of ammonia. Later, we investigated the effect of

support using 5Ni5Ag. CeO<sub>2</sub> found to be effective support for ammonia synthesis. We characterized monometallic (Ni or Ag) and bimetallic (NiAg) to understand the difference in their activity.

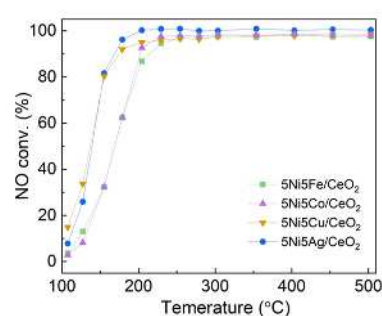


Figure 1. NO conversion using bimetallic catalysts

XRD analysis revealed that Ni and Ag metal were in metallic state in all three catalysts. H<sub>2</sub>-TPR profile of Ag/CeO<sub>2</sub> showed Ag<sub>2</sub>O oxide was reduced at 172 °C which shifted to higher temperature (193 °C) in bimetallic NiAg catalyst. Ni/CeO<sub>2</sub> showed reduction at 453 °C which shifted to lower temperature (279 °C). CO-chemisorption showed metal dispersion was higher in bimetallic than monometallic catalysts.

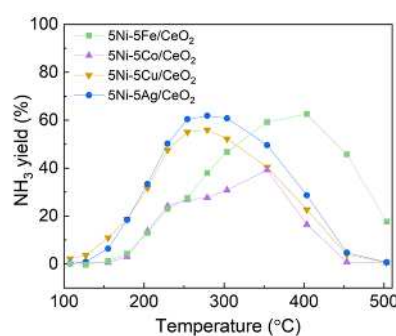


Figure 2. Ammonia yield using bimetallic catalysts

In summary, 5Ni5Ag/CeO<sub>2</sub> catalyst exhibited high activity for NTA reaction.

<sup>1</sup>K. Kobayashi, R. Atsumi, Y. Manaka, H. Matsumoto, T. Nanba, *Catal. Sci. Technol.*, **9**, 289 (2019)

# Plasmon-assisted hydrogenation and dehydrogenation reactions of noble metal nanoparticles

(Shizuoka University<sup>A</sup> · Osaka University<sup>B</sup>) ○Priyanka Verma<sup>A</sup> · Kohsuke Mori<sup>B</sup> · Yasutaka Kuwahara<sup>B</sup> · Ryo Watanabe<sup>A</sup> · Hiromi Yamashita<sup>B</sup> · Choji Fukuhara<sup>A</sup>

## 1. Introduction

The localized surface plasmon resonance (LSPR) mediated enhanced chemical activity can be entitled as a promising strategy for efficient solar to chemical energy conversion.<sup>1</sup> To tune the selectivity of a desired product in a chemical reaction is of paramount importance yet a great challenge. Herein, a new strategy to effectively enhance the selectivity of the product formation under visible light irradiation is reported.<sup>2</sup> A series of Ag catalysts deposited on metal oxide support materials (TiO<sub>2</sub>, ZrO<sub>2</sub>, Al<sub>2</sub>O<sub>3</sub> and CeO<sub>2</sub>) along with their preparative techniques, optimum metal content ratio and effect of different wavelength of light is explored for the chemoselective reduction of *p*-nitrostyrene to *p*-aminostyrene under visible light irradiation.

## 2. Experimental

The catalyst was prepared by a simple impregnation method. 500 mg of metal oxide support materials (TiO<sub>2</sub>, ZrO<sub>2</sub>, CeO<sub>2</sub> and Al<sub>2</sub>O<sub>3</sub>) and sodium laurate (5 mg) was dispersed and ultrasonicated in 100 mL ethanol solution. The mixture was bubbled with argon gas in order to maintain inert atmosphere. Subsequently desired amount of aqueous AgNO<sub>3</sub> solution was added into the mixture and stirred continuously for 6 h. The suspension was evaporated under vacuum and the obtained powder was dried overnight at 80 °C. The obtained sample was named as Ag/M<sub>x</sub>O<sub>y</sub> and series of catalysts with varied amount of Ag (0.5, 1.0, 2.0 and 5.0 wt. %) were prepared.

## 3. Results and Discussion

The prepared catalysts were characterized by a range of physicochemical techniques including UV-vis, transmission electron microscopy (TEM) and X-ray photoelectron spectroscopy (XPS). All samples exhibited the strong intrinsic plasmon peak at around 400 nm, attributing to the LSPR effect of Ag NPs. A single broad peak absorption suggests the spherical morphology of the prepared NPs which was further confirmed by TEM. The LSPR peak maximum was observed at 516, 450, 463, 430 nm for Ag/TiO<sub>2</sub>, Ag/CeO<sub>2</sub>, Ag/ZrO<sub>2</sub> and Ag/Al<sub>2</sub>O<sub>3</sub>, respectively. The Ag/TiO<sub>2</sub> absorption peak was found to be significantly red shifted in comparison to other catalysts. The average particle size of Ag/TiO<sub>2</sub>, Ag/ZrO<sub>2</sub>, Ag/Al<sub>2</sub>O<sub>3</sub> and Ag/CeO<sub>2</sub> was found out to be 11.8 ± 3.4, 6.84 ± 2.1, 20.7 ± 5.2 and 9.0 ± 3.2 nm, respectively.

The chemoselective reduction reaction was carried out in ethanolic suspension at room temperature and pressure utilizing ammonia borane (AB) as an in-situ source of H<sub>2</sub>.

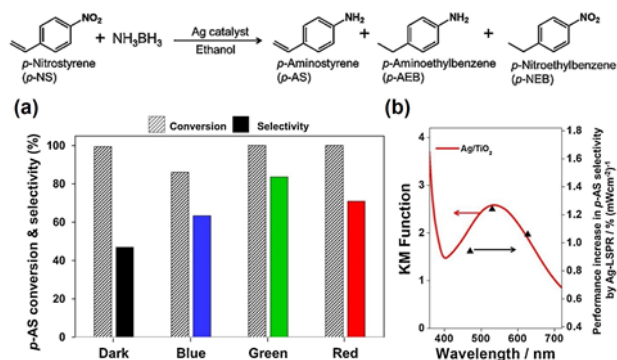


**Figure 1.** (a) Effect of using different wavelengths of light (power = 66.7 mW) in the reaction conversion and selectivity utilizing Ag/TiO<sub>2</sub> (b) wavelength of performance increase in the *p*-AS selectivity over Ag/TiO<sub>2</sub> using LED light.

All catalysts displayed complete conversion with varied selectivity obtained for different catalysts. Under light irradiation conditions, the kinetics and overall selectivity was found to be significantly enhanced. Amongst all, Ag/TiO<sub>2</sub> displayed a maximum chemoselectivity of 81 % shown by Ag/TiO<sub>2</sub> under light irradiation conditions.

In order to have a detailed insight of the mechanism and absorption of light by plasmonic Ag NPs, the reactions on Ag/TiO<sub>2</sub> with LED light of different wavelengths and comparison of the obtained results in dark and under visible light irradiation conditions ( $\lambda > 420$  nm) was reported (Figure 1a). The LED and their corresponding wavelengths employed in the present study are Blue (470 nm), Green (530 nm) and Red (627 nm). The order of catalytic activity follows the trend Green LED > Red LED > Blue LED > Dark conditions. The selectivities changed significantly upon varying the source of monochromatic LED light. The green LED was found to be the most effective amongst all. Figure 1 (b) summarizes the action spectrum in the performance increase over Ag/TiO<sub>2</sub> catalyst using monochromatic light. The increasing rate of catalytic performance activities was found to be highly consistent with the LSPR absorption intensity of Ag NPs. This result concludes that LSPR plays an important role in increasing the *p*-AS selectivity under light irradiation conditions. We hope that such plasmonic photocatalysts will assist in opening a new promising avenue in the visible-light-driven heterogeneous catalysis.

## References

- 1) P. Verma, K. Mori, Y. Kuwahara, R. Raja, H. Yamashita, *Mater. Adv.*, 2, 880 (2021).
- 2) P. Verma, Y. Kuwahara, K. Mori, H. Yamashita, *Catal. Today*, 324, 83 (2019).

## Effect of Ca addition on the catalytic activity of BaTiO<sub>3</sub> for oxidative coupling of methane

(Nagoya Institute of Technology) ○ GAN Rongguang, NISHIDA Yoshihide, HANEDA Masaaki

### 1. Introduction

Oxidative coupling of methane (OCM) reaction has attracted extensive attention due to its energy-saving and convenience process [1]. Although perovskite-type catalysts with high thermal stability are known to show the activity for OCM reaction, the C<sub>2</sub> yield is not high enough for industrial use due to the low activity and selectivity [2]. In this study, we investigated the additive effect of Ca on the catalytic performance of BaTiO<sub>3</sub> and found that the addition of small amount of Ca is effective to increase the C<sub>2</sub> yield. The detail experiments were performed to reveal the role of Ca.

### 2. Experimental

Catalysts were prepared by conventional impregnation method. Commercial BaTiO<sub>3</sub> powder was immersed with an aqueous solution of Ca(NO<sub>3</sub>)<sub>2</sub>·4H<sub>2</sub>O, followed by evaporation to remove water. The obtained powders were dried at 110 °C and calcined at 900 °C for 8 h in air. The loading of Ca was set to 1 ~ 30 wt%. The catalytic activity was evaluated using a flow reactor system. Catalyst (100 mg) was loaded into a tubular quartz reactor, and a gas mixture of CH<sub>4</sub>/O<sub>2</sub>/N<sub>2</sub> (20/5/20 mL/min) was introduced to the reactor. The steady-state activity was evaluated by analyzing the reaction/product gases with gas chromatography. As for the catalyst characterizations, XRD, BET surface area and O<sub>2</sub>-TPD were carried out.

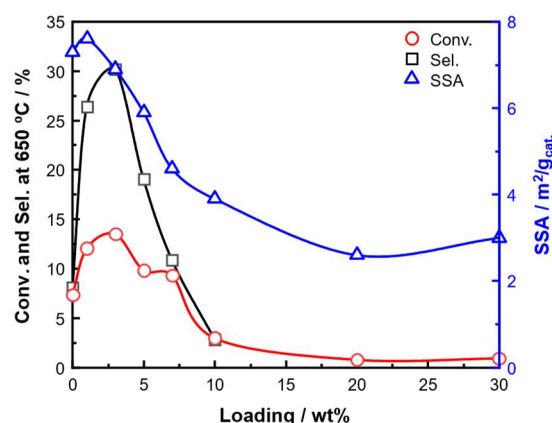
### 3. Results and Discussion

Fig. 1 shows the effect of Ca loading on the catalytic performance (CH<sub>4</sub> conversion, C<sub>2</sub> selectivity) of Ca-doped BaTiO<sub>3</sub> for OCM reaction at 650 °C. Not only CH<sub>4</sub> conversion but also C<sub>2</sub> selectivity were increased by addition of Ca up to 3 wt%. However, further increase in Ca loading caused a decrease in the activity. In Fig.1 is also shown the change in BET surface area as a function of Ca loading. Basically, BET surface area was gradually decreased with increasing Ca loading suggesting that BET surface area is not an important factor determining the catalytic activity of Ca-doped BaTiO<sub>3</sub>.

In the range of Ca loading below 3 wt%, only the XRD peaks due to BaTiO<sub>3</sub> were observed. However, increase in the Ca loading up to 5 wt% caused an appearance of new peaks due to BaCaTiO<sub>4</sub>, indicating the solid phase reaction between Ca additive and BaTiO<sub>3</sub>. From the comparison with the catalytic performance shown in Fig.1, the formation of BaCaTiO<sub>4</sub> is negative effect on the catalytic performance of BaTiO<sub>3</sub>.

In order to obtain an information on the role of Ca additive, O<sub>2</sub>-TPD profiles from Ca-doped BaTiO<sub>3</sub> were measured. O<sub>2</sub> desorption from BaTiO<sub>3</sub> was found to be increased by the addition of Ca. The maximum amount of O<sub>2</sub> desorption was achieved for 3 wt% Ca-doped BaTiO<sub>3</sub>. This is in agreement with the order of C<sub>2</sub> yield, suggesting that the Ca additive promotes the oxygen mobility on the surface of BaTiO<sub>3</sub>. More detail experiments to discuss the promotional effect of Ca is now in progress.

This research is supported by CSC fundament.



**Fig.1.** Dependence of CH<sub>4</sub> conversion, C<sub>2</sub> selectivity for OCM reaction at 650 °C and BET surface area on Ca loading.

- 
- 1) J.H. Lunsford, *Angew. Chem. Int. Ed.*, 34, 970-980 (1995).
  - 2) L. Bai, F. Polo-Garzon, Z.H. Bao, S. Luo, B.M. Moskowit, H. Tian, Z.L. Wu, *ChemCatChem*, 11, 2107-2117 (2019).

# CO<sub>2</sub> hydrogenation reaction over Pd-containing MWW zeolite catalyst

(Tokyo Inst. Tech.) ○Willie Yang, Shuhei Yasuda, Sridharan Balu, Muyuan Yu, Toshiki Kaseguma, Toshiyuki Yokoi

## 1. Introduction

Different from the well-known ZSM-5 (MFI) catalyst, the MCM-22 (MWW) possesses three pore systems: the two-dimensional sinusoidal channels composed of slightly elliptical 10-MR, the characteristic of 12-MR supercages accessible through 10-MR windows, and pockets on its external surface [1]. Due to the distinctive pore structure, the MCM-22 zeolite has shown robust reaction performance in many catalytic processes such as MTO reaction. The group also consider this zeolite catalyst a potential support for CO<sub>2</sub> hydrogenation. Here in this work, the Pd-containing MWW zeolite catalyst has been deployed for the CO<sub>2</sub> hydrogenation reaction.

## 2. Experimental

A series of MWW typed aluminosilicate zeolite, MCM-22, were synthesized as the following method. First, the as-calcined sample was synthesized through hydrothermal synthesis at 150 °C from an aqueous gel of 1.0 SiO<sub>2</sub> : 0.15 Na<sub>2</sub>O : 0.025 Al<sub>2</sub>O<sub>3</sub> : 0.9 hexamethylenimine (HMI) : 45 H<sub>2</sub>O mol composition [1]. Then the ammonium-type, proton-type, and sodium-type sample were obtained through ion exchange and calcination. Finally, the 1 wt% of Pd was impregnated into the zeolite support by wet impregnation method. The final samples were obtained with the nomenclature of Pd/[M]-MWW-10 where and [M] represents the containing charge balance cations.

## 3. Results and discussion

From the XRD results, the patterns of MCM-22 and Pd-containing MCM-22 are nearly identical. However, the diffraction peak attributed to PdO (101) particles was observed. The SEM images revealed the well-defined layered

morphology. Furthermore, the elemental compositions measured from EDX agreed well with the ICP-AES results.

To investigate the intrinsic molecular interactions between adsorbates and the catalyst statically and dynamically, the *in-situ* DRIFT measurements were performed. The sample was pre-treated in 20vol%H<sub>2</sub>/N<sub>2</sub> at 400 °C for 1 hour. In Figure 1, chemisorption of CO<sub>2</sub> on the Pd/MWW-10 samples with different Na contents were detected differently under the flow of 20vol%CO<sub>2</sub>/H<sub>2</sub> at 250 °C. The band around 1640 cm<sup>-1</sup> of Pd/MWW-10 and Pd/Na-MWW-10 is considered as the carbonate species resulting from the sodium cations and trace amount of water molecules from aluminum-rich zeolites [2]. The dynamic evolution of intermediate species was also observed. During CO<sub>2</sub> hydrogenation, carbonate (1520 cm<sup>-1</sup>), bicarbonate (1640 cm<sup>-1</sup>), formate (1603 cm<sup>-1</sup>), and CO (1800– 2100 cm<sup>-1</sup>) were identified as the key intermediates [3]. In the three samples, band related to each intermediates obtained different intensities implying a distinctive reaction pathways from each sodium content observed from DRIFT spectra. Thus, it can be concluded that the reaction mechanism can be controlled by the adsorbate species and the relative position and the amount of sodium cations and Pd particles.

## References:

- 1) Wang, Y., et al, *Journal of Catalysis*, 333, 17-28. (2016).
- 2) Cheung, O., et al, *ACS omega*, 5(39), 25371-25380 (2020).
- 3) Feng, K., et al, *Journal of Energy Chemistry*, 62, 153-171. (2021).

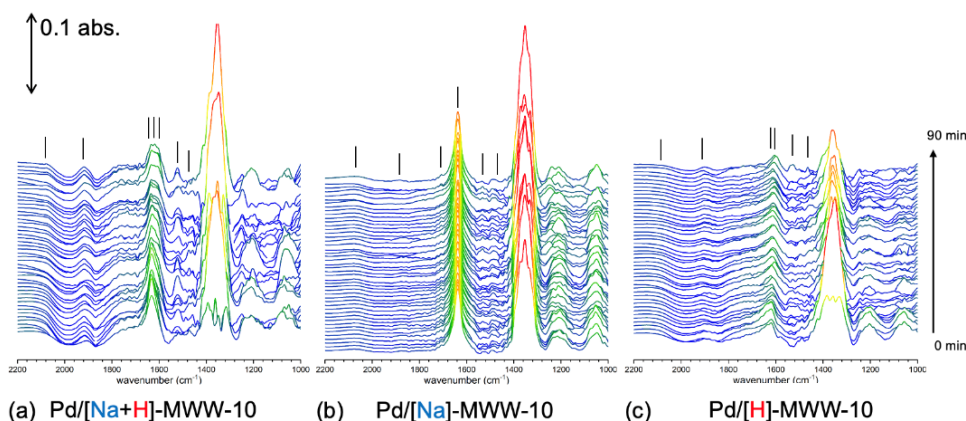


Figure 1 In-situ DRIFT measurements of the Pd-containing MWW zeolite catalysts under CO<sub>2</sub>+H<sub>2</sub> gas flow at 250°C.

International sess.

## [2F05-2F07] International sess. (5)

Chair:Ryo Watanabe(Shizuoka Univ.)

Fri. Oct 28, 2022 10:15 AM - 11:15 AM Room-F (13A Conf. room)

---

### [2F05] Direct synthesis of carbamates as polyurethane raw materials from low-concentration of CO<sub>2</sub> equivalent to thermal power plant exhaust gas

○Hiroki Koizumi<sup>1</sup>, Katsuhiko Takeuchi<sup>1</sup>, Kazuhiro Matsumoto<sup>1</sup>, Norihisa Fukaya<sup>1</sup>, Kazuhiko Sato<sup>1</sup>, Masahito Uchida<sup>2</sup>, Seiji Matsumoto<sup>2</sup>, Satoshi Hamura<sup>2</sup>, Jun-Chul Choi<sup>1</sup> (1. National Institute of Advanced Industrial Science and Technology, 2. Tosoh Corporation)

10:15 AM - 10:30 AM

### [2F06] Design of efficient catalyst for higher alcohols synthesis via CO<sub>2</sub> hydrogenation

○Minghui Zhao<sup>1</sup>, Nozomi Kawamoto<sup>1</sup>, Kenji Kamiya<sup>1</sup>, Eika W. Qian<sup>1</sup> (1. Tokyo University of Agriculture and Technology)

10:30 AM - 10:45 AM

### [2F07] [Invited] Oxidative coupling of methane over alkaline tungstate catalysts

○Kazuhiro Takanabe<sup>1</sup> (1. The University of Tokyo)

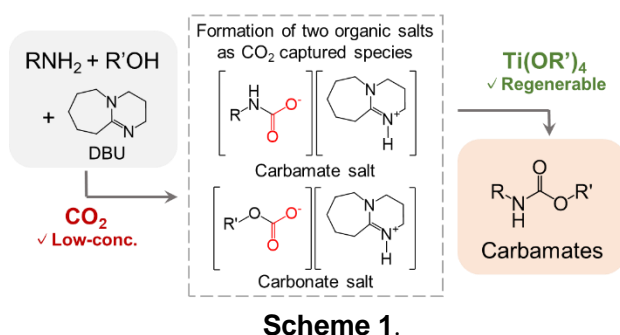
10:45 AM - 11:15 AM

## Direct synthesis of carbamates as polyurethane raw materials from low-concentration of CO<sub>2</sub> equivalent to thermal power plant exhaust gas

(AIST\*, Tosoh Corporation\*\*) ○Hiroki Koizumi\*, Katsuhiko Takeuchi\*, Kazuhiro Matsumoto\*, Norihisa Fukaya\*, Kazuhiko Sato\*, Masahito Uchida\*\*, Seiji Matsumoto\*\*, Satoshi Hamura\*\*, Jun-Chul Choi\*

### 1. Introduction

In the technologies of carbon dioxide (CO<sub>2</sub>) capture and utilization (CCU), the usage of CO<sub>2</sub> as a C1 source for organic syntheses is one effective approach to achieve CO<sub>2</sub> emission reduction. Among synthesizable compounds from CO<sub>2</sub>, carbamates (RNHC(O)OR') are attractive because those can be converted into isocyanates as monomers of polyurethanes, which are widely used for such as automobile parts. We have reported synthesis of carbamates from CO<sub>2</sub> using amines and environmental-friendly regenerable reagents, Ti(OR')<sub>4</sub> or Si(OR')<sub>4</sub>. Although these methods can provide high selectivity and high yields of carbamates, high-purity and high-pressure (~3.0 MPa at room temperature) of CO<sub>2</sub> are essential. In contrast, direct utilization of low-concentration and low-purity CO<sub>2</sub> such as exhaust gas of fire power plants is one ideal method owing to excluding energy-loss processes in purification, condensation, and compression. Therefore, we designed direct synthetic method of carbamates from low-concentration of CO<sub>2</sub> by the combination of regenerable reagent Ti(OR')<sub>4</sub> and CO<sub>2</sub> capture methods using 1,8-diazabicyclo[5.4.0]undec-7-ene (DBU), which induces formation of two organic salts as CO<sub>2</sub> captured species: carbamate salt formed from amine with DBU and carbonate salt formed from alcohol with DBU (Scheme 1.)<sup>[1]</sup>.



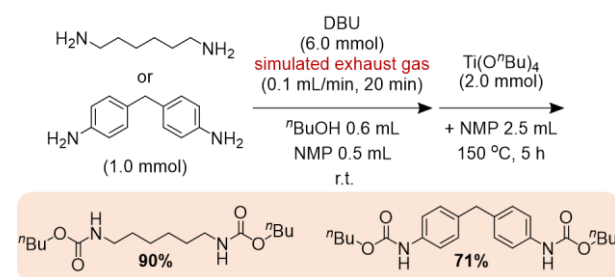
### 2. Experimental

First, to capture CO<sub>2</sub> into a reaction solution as the two organic salts as shown in Scheme 1, 0.5 mL of NMP solution containing 2.0 mmol of monoamine or 1.0 mmol of diamine, 6.0 mmol of DBU, and 0.6 mL of

<sup>n</sup>BuOH was bubbled by low-concentration of CO<sub>2</sub> for 20 min at 0.1 L/min in a stainless reactor (volume: 6 mL). Then, additional 2.5 mL of NMP and 2.0 mmol of Ti(O<sup>n</sup>Bu)<sub>4</sub> were added to the reaction mixture. The reaction vessel was tightly sealed by a stainless lid with a gasket and then heated in an oil bath at 150 °C for 5 h. Yields of carbamates were determined by <sup>1</sup>H NMR using 1,3,5-trimethylbenzen as the internal standard.

### 3. Results and Discussion

Various carbamates were obtained in moderate to high yields by the reaction of Ti(O<sup>n</sup>Bu)<sub>4</sub> with the two organic salts formed from 15 vol%CO<sub>2</sub> (CO<sub>2</sub>:N<sub>2</sub> = 15:85, v/v). Conducting the control experiments and the determination of amounts of captured CO<sub>2</sub> into the organic salts, we clarified that the yields of carbamates were correlated with the amounts of captured CO<sub>2</sub>. The simultaneous formation of two organic salts was important to obtain the high yield of carbamates owing to increasing the amount of captured CO<sub>2</sub>. This synthetic method could be applied to use of simulated exhaust gas (CO<sub>2</sub>: 15 vol%, CO: 300 ppm, NO<sub>2</sub> and SO<sub>2</sub>: 500 ppm, N<sub>2</sub>: balanced), which is equivalent to exhaust gas of coal fired power plants including impurities. Using this simulated exhaust gas, dicarbamates as important precursors of industrially useful alkyl and aryl diisocyanates were obtained in 90% and 71% yields, respectively (Scheme 2).



*Acknowledgement:* This work is supported by NEDO Feasibility Study Program (Uncharted Territory Challenge 2050).

*Reference:* [1] H. Koizumi *et al.*, *ACS Sustainable Chem. Eng.* **2022**, 10, 5507.

## Design of efficient catalyst for higher alcohols synthesis via CO<sub>2</sub> hydrogenation

(Tokyo University of Agriculture and Technology\*) ◯Minghui Zhao\*,  
Nozomi Kawamoto\*, Kenji Kamiya\*, Eika W. Qian\*

### 1. Introduction

Directly synthesis of higher alcohols (HAs) via CO<sub>2</sub> hydrogenation has attracted considerable attention. However, suffered from the complicated kinetics and adverse thermodynamic properties, the poor yield of target product makes this route industrialization challenging. Hence, the development of an efficient catalyst for this reaction is of great importance. Considered from the perspective of sustainable and large-scale application, Co-based catalysts deserve more attention [1]. Meanwhile, the morphology of a catalyst also has influence on the catalytic performance and thus has been widely studied. Mesoporous metal oxides have been utilized due to the unique pore structure which could act as the channel to expose more active site and provide microenvironment conditions as nanoreactor [2]. In this work, we selected non-precious mesoporous cobalt based catalyst as the research subject. The MOF was utilized as a template for the catalyst synthesis. Also, the effect of alkali metal, the carbonization temperature and the promoter have been studied in this work.

### 2. Experimental

The catalysts were synthesized by using MOF as template which refers to build MOF containing target metal and calcinated under suitable condition. The catalytic performance of HAs production directly via CO<sub>2</sub> hydrogenation were then examined using a fixed-bed pressurized flow reaction system under the following conditions: 200 - 300 °C, 3 - 5 MPa, GHSV of 5000 h<sup>-1</sup> and H<sub>2</sub>/CO<sub>2</sub> ratio of 3. The effects of morphology and promoter on the performance of catalysts were characterized by N<sub>2</sub> adsorption, X-ray photoelectron spectroscopy (XPS), and Temperature-programmed reduction (TPR).

### 3. Results and Discussion

The effect of promoter, the amount of potassium doping and the carbonization temperature

were studied in this work. Compared with the catalyst promoted by Ni, the Fe promoted catalyst exhibited a relatively high chain-growth probability. This could be ascribed to the appearance of FeC<sub>x</sub> introduced by Fe metal. The HAs selectivity of catalyst with 0.5% K content increased to 2% which maybe explained by the electron transformation from K to Cobalt. As for the effect of carbonization temperature, as shown in fig.1, the catalyst carbonized at 400 °C possessed the best performance. The conversion rate and the selectivity to HAs both increased. This could be ascribed to the suitable amount of carbides appearing during the carbonization process.

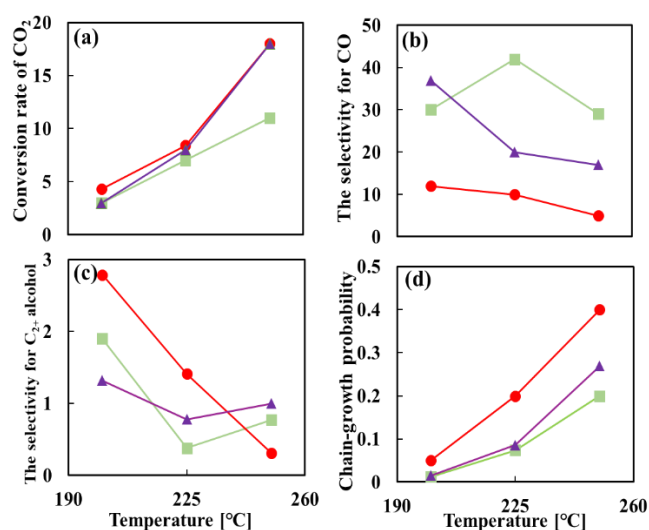


Fig.1 (a) CO<sub>2</sub> conversion (b) Selectivity of CO (c) Selectivity of HAs alcohol (d) chain growth probability of catalyst carbonization at different temperature as a function of temperature. Calcinated at —■— 300 °C, —●— 400 °C, —▲— 500 °C.

[1] Xu et al., Advances in Higher Alcohol Synthesis from CO<sub>2</sub> Hydrogenation, Chem 2021; 7(4): 849.

[2] Zeng et al., Catalysts design for higher alcohols synthesis by CO<sub>2</sub> hydrogenation: Trends and future perspectives. Applied Catalysis B: Environmental 2021; 291 (2021): 120073.

## Oxidative coupling of methane over alkali tungstate catalysts

(Univ. Tokyo) OKazuhiro Takanabe

The oxidative coupling of methane (OCM) is a promising direct route to make C<sub>2</sub> products from CH<sub>4</sub> using cofed O<sub>2</sub>. It is generally agreed that the OCM process proceeds via a complex reaction network involving surface-catalyzed radical formation and its chain reaction in the gas phase.<sup>1,2</sup>

Among many investigated catalysts for OCM, Mn-containing Na-tungstate containing catalysts exhibit excellent performance in the OCM. We discovered that the promotional effects on both rate and selectivity were attained over the catalyst in the presence of H<sub>2</sub>O, which is one of the major products.<sup>3</sup> On detailed microkinetic analysis study, it appears that the OH radical from reaction of O<sub>2</sub> and H<sub>2</sub>O plays a key role in improving the performance. After composite variation, Mn species as a catalyst component is not essential for this OH-radical pathway although its presence is effective to improve the overall rate.<sup>5</sup> The study also confirms that the tungstate is among the most effective anions as they hold the alkali active sites at high temperatures without possessing redox properties that combust hydrocarbons.<sup>5</sup>

Over the Na<sub>2</sub>WO<sub>4</sub>/SiO<sub>2</sub> catalyst, we identified that active components are alkali metal existing at the most outer surface, which forms peroxide

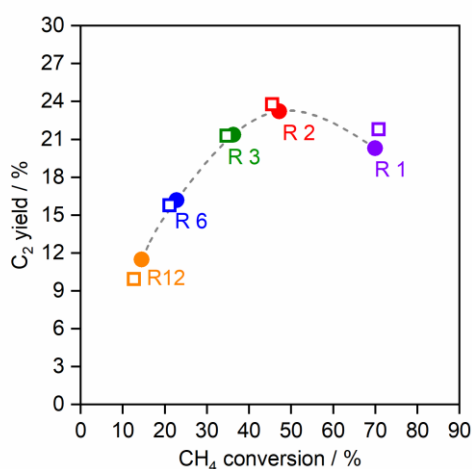
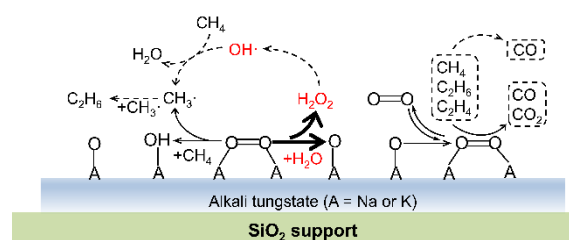


**Figure 1.** C<sub>2</sub> yield of OCM reaction as a function of CH<sub>4</sub> conversion with 5 wt% K<sub>2</sub>WO<sub>4</sub>/SiO<sub>2</sub> (filled circle) and 5 wt% Na<sub>2</sub>WO<sub>4</sub>/SiO<sub>2</sub> (open square) under different R: CH<sub>4</sub>/O<sub>2</sub> ratio (0.8 g K<sub>2</sub>WO<sub>4</sub>/SiO<sub>2</sub> or 0.6 g Na<sub>2</sub>WO<sub>4</sub>/SiO<sub>2</sub>, 850 °C, CH<sub>4</sub> 10 kPa, O<sub>2</sub> 0.83-10 kPa, H<sub>2</sub>O 1.7 kPa, total pressure 101 kPa, Ar balance).

species in equilibrium with gas-phase oxygen, evident by the near-ambient pressure X-ray photoelectron spectroscopy (NAP-XPS).<sup>6</sup> This surface peroxide is likely responsible for OH radical formation to selectively convert CH<sub>4</sub> to C<sub>2</sub>, well consistent with the previous kinetic results.<sup>4</sup>

Although Na<sub>2</sub>WO<sub>4</sub>-based catalysts suffer from melting at the OCM operating condition, K<sub>2</sub>WO<sub>4</sub>-based catalysts maintain its crystal forms, which may have benefit for long-term durability.<sup>7</sup> After optimization, we discovered that the similar maximum C<sub>2</sub> yields can be achieved using K<sub>2</sub>WO<sub>4</sub>/SiO<sub>2</sub> to those using Na<sub>2</sub>WO<sub>4</sub>/SiO<sub>2</sub>, as shown in **Figure 1**.<sup>7</sup> Very similar promotional effects of H<sub>2</sub>O were identified by kinetic analysis, suggesting the OH-radical mediated pathway as proposed in **Scheme 1**. The surface species in situ is indeed evident by NAP-XPS for the K<sub>2</sub>WO<sub>4</sub>/SiO<sub>2</sub>, identifying K-peroxide or K-superoxide formation during the OCM condition.<sup>7</sup> Common reaction pathway is thus proposed for Na-based, and K-based catalysts with H<sub>2</sub>O effects.



**Scheme 1.** Schematic drawing of common surface reaction steps involved in OCM over alkali (Na, K) tungstate catalysts.

## Reference

- Lunsford, J.H., *Angew. Chem.*, 34, 970 (1995).
- Labinger, J.A., Ott, K.C., *J. Phys. Chem.* 91, 2682 (1987).
- Takanabe, K., Iglesia, E., *Angew. Chem. Int. Ed.* 47, 7689 (2008).
- Takanabe, K., Iglesia, E., *J. Phys. Chem. C* 113, 10131 (2009).
- Liang, Y., Li, Z., Nourdine, M., Shahid, S., Takanabe, K., *ChemCatChem*, 6, 1245 (2014).
- Takanabe, K., Khan, A.M., Tang, Y., Nguyen, L., Ziani, A., Jacobs, B.W., Elbaz, A.M., Sarathy, S.M., Tao, F.F., *Angew. Chem. Int. Ed.* 56, 10403 (2017).
- Li, D., Yoshida, S., Siritanaratkul, B., Garcia-Esparza, A., Sokaras, D., Ogasawara, H., Takanabe, K., *ACS Catal.* 11, 14237 (2021).